



Efficient voltage actuators based on rapid heat and electric dual-response poly(aryl ether ketone) shape memory composites reinforced with radially aligned CNTs

Shuai Yang^a, Yang He^a, Yanju Liu^b, Jinsong Leng^{a,*}

^a Center for Composite Materials and Structures, Harbin Institute of Technology, Harbin, PR China

^b Department of Astronautic Science and Mechanics, Harbin Institute of Technology, Harbin, PR China

ARTICLE INFO

Keywords:

- A. Carbon nanotubes and nanofibers
- A. Polymer-matrix composites (PMCs)
- B. Directional orientation
- A. Smart materials

ABSTRACT

In this paper, we synthesized the shape memory poly(aryl ether ketone) (PAEK) and fabricated the radially oriented CNTs enhanced PAEK composite actuators. The introduction of highly aligned CNTs endowed PAEK matrix great thermal stability, good mechanical properties, and excellent shape memory effect. The formation of CNTs conductive path in PAEK matrix was instrumental in improving thermal and electrical conductivity, promoting efficient heat/electric dual triggered shape memory effect with high recovery ratio, rapid shape recovery and low triggering voltage. In addition, we used aligned CNTs/PAEK composites with 15 wt% CNTs as voltage actuators, and designed the two kinds of voltage actuators (angle-mode and time-mode) to achieve the different actuating actions via the applied voltage (range from 8 V to 50 V). These efficient composite voltage actuators exhibited the excellent stability and durability in continuous voltage actuating, which were expected to open door for smart actuators and electronic devices.

1. Introduction

The developments and advancements in research of smart and rapid responsive actuating materials strive to meet the requirements of smart actuators, which could be widely utilized in electronic devices, biomedical devices, and aerospace applications, etc [1,2]. Shape memory polymers (SMPs), as a kind of responsive smart materials, could be programmed to temporary shape via the external conditions (temperature and force), and recover to permanent shape under certain stimulus, such as heat [3], electric [4], light [5], magnetism [6], solvent [7], humidity [8], and pH [9] etc. Due to the unique deformation-recovery capability, SMPs have various advantages of programming rigidity and low cost, which are used in myriad fields: tissue engineering, artificial muscle, smart actuators, and aerospace components, etc [10–12]. Generally, shape memory effect (SME) originates from the internal net points and switching segment. Crystalline phase and physically or covalently cross-linked regions act as net points, which could memorize the permanent shape and recover to it. The stability is necessary for the fixed net points, ensuring the stable shape upon the high temperature. Flexible segments and amorphous regions act as the switching segment,

which could deform undergoing the high temperature and applied external forces. Besides, they could retain the deformed shape while keeping force and decreasing temperature. When the temperature reached above transition temperature again, the switching segments are actuated and begin to move. Macroscopically, the SMPs recover to the permanent shape [13,14].

Nevertheless, SMPs exhibit several disadvantages such as poor mechanical properties, low response speed, and weak strength [15], which largely limit their diverse applications. Commonly, the mechanical performances of SMPs could be improved mainly by two methods [16,17]: Combining shape memory polymers with strengthened and elastic materials, such as silicon elastomer [18]; in addition to dope reinforcing fillers such as carbon nanotubes (CNTs) [19], carbon fibers [20], and Fe₃O₄ particles [21], etc. Due to the easy processing and enhanced performances, the integration of reinforcing fillers is more commonly used for the preparation of enhanced shape memory composites. In addition, reinforcing fillers commonly possess the certain functionality which could endow SMPs with unique performances and diverse stimulated modes. Conventional SMPs almost belong to heat-driven SMPs, which triggered by heating. Magnetocaloric effect of

Abbreviations: PAEK, Poly(aryl ether ketone); CNTs, Carbon nanotubes; SMPs, Shape memory polymers.

* Corresponding author.

E-mail address: lengjs@hit.edu.cn (J. Leng).

<https://doi.org/10.1016/j.compositesa.2022.106940>

Received 5 October 2021; Received in revised form 12 March 2022; Accepted 24 March 2022

Available online 26 March 2022

1359-835X/© 2022 Elsevier Ltd. All rights reserved.

Fe_3O_4 particles endows SMPs with magnetic-actuated shape recovery behaviors [22]. The incorporation of CNTs into SMPs matrix could render electric- and light-triggered SME due to the electrothermal and photothermal effect of CNTs [23]. Among the various triggering modes, electric actuation has attracted much attentions due to the convenient manipulation and low cost [24,25]. To fulfill the electric-actuated SME, constructing the conductive path in SMPs matrix is necessary, in addition that CNTs are most usually employed as the conductive fillers to construct the whole path [26]. Due to the axial tubular characteristic of CNTs, the reinforced mechanical properties and conductivity are closely related to the distribution and orientation of CNTs in SMPs matrix. With the simple fabrication techniques (physical blending or filling), reinforcing CNTs are difficult to evenly distribute or radially distribute in SMPs matrix [27]. The dispersion and orientation of fillers in matrix is also a major subject in the preparation of fillers enhanced composites.

Poly(aryl ether ketone) (PAEK), as a universal engineering thermoplastic, possesses excellent mechanical properties, thermal stability, and chemistry resistance, which expanding to the diverse application fields in aerospace, engineering industry, and energy storage [28–30]. In addition, the rigid structures and flexible chains could be adjusted through the variation of monomers and the integration of other side chains or groups, for the fulfillment of shape memory effect. Herein, we proposed a synthesis route of PAEK to achieve the excellent SME. To obtain the reinforced mechanical properties and excellent electric-actuated SME, CNTs were integrated into PAEK matrix to fabricate heat/electric dual triggered shape memory composite actuators. It was worth noting that the oriented distribution of CNTs in PAEK matrix was achieved through an electro-mixed fusion preparation method. Radially aligned CNTs endowed composites with the enhanced strength and great conductivity, promoting the efficient heat/electric dual triggered shape recovery behaviors. In addition, we employed aligned CNTs/PAEK composites as the voltage actuators, and designed two kinds of voltage actuating modes (angle-mode and time-mode) to achieve diverse actuating actions of applied voltage (range from 8 V to 50 V). These efficient composite voltage actuators exhibited the excellent stability and durability in continuous voltage actuating tests, which exhibited the great using potential in smart actuators.

2. Experimental

2.1. Materials

4,4'-(hexafluoroisopropylidene) diphenol, 4,4'-difluorobenzophenone, potassium carbonate (K_2CO_3), and tetramethylene sulfone (TMSF) were bought from Aladdin Industrial. Toluene and N-methyl kelopyrrolidide (NMP) were all supplied by Tianjin Guangfu Chemical Reagent Factory. Multiwall CNTs were bought from Chinese Academy of Sciences, Chengdu Organic Chemistry Co., Ltd.

2.2. Synthesis of PAEK

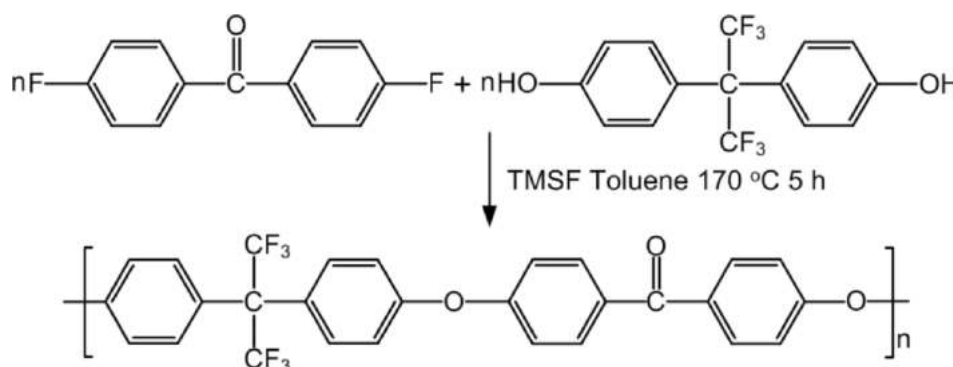
PAEK was synthesized by nucleophilic substitution using the following polymerization procedure, as depicted in Scheme 1. A certain proportion of 4,4'-(hexafluoroisopropylidene) diphenol, 4,4'-difluorobenzophenone, and K_2CO_3 were carefully added into the TMSF/toluene mixed solvent, in addition that Dean-Stark trap and nitrogen atmosphere were equipped. The mixture was thoroughly stirred, and the temperature was increased to 140 °C for 2 h to remove water. During the reaction process, toluene was used as the azeotropic solvent. Afterwards, the temperature was increased to 170 °C for 3 h to distill the toluene and carry out the polymerization. After polymerization, the viscous product was slowly poured into a beaker containing isopropanol and distilled water. Finally, the precipitate was filtered and rinsed with distilled water for several times to remove solvents, unreacted monomers, and oligomers. The synthesized PAEK was dried at 40 °C under vacuum for 24 h and the yield was 91%.

2.3. Preparation of oriented CNTs enhanced PAEK composites

Oriented CNTs enhanced PAEK composites were fabricated through an electro-mixed fusion process.²⁷ PAEK was dissolved into NMP and stirred to obtain the homogeneous solution. Certain amounts of CNTs were added into PAEK solution, and further stirred until the formation of PAEK/CNTs homogeneous mixed dispersion. Subsequently, the PAEK/CNTs mixed dispersion was poured into a homemade mould, equipped with conductive foils in the two sides, which connected with applied external voltage. Then, certain voltage was applied for 2 min to orientate CNTs. Afterwards, the mixture was dried at 80 °C for 48 h. Finally, prepared PAEK/CNTs composites were peeled off from the mould and stored carefully for testing. The fabrication process is illustrated in Fig. 1, and different content of CNTs and applied voltages for CNTs orientation were performed to fabricate PAEK/CNTs composites, recorded in Table 1.

2.4. Characterization

^1H -nuclear magnetic resonance (^1H NMR) spectra was obtained from an ADVANCE III 400 MHz 010601 spectrometer (Bruker). CDCl_3 was used as the solvent and tetramethylsilane (TMS) was used as the internal reference. Fourier transform infrared (FTIR) spectroscopy was recorded over the frequency range of 4000–400 cm^{-1} with a resolution of 4 cm^{-1} by a Spectrum Two (PerkinElmer). Wide-angle X-ray diffraction (WAXD) patterns were performed on an X'pert XRD analyzer (Panalytical B.V.). The range of 2θ was 5–55°, and the step size was 10°/min. Differential scanning calorimetric (DSC) curves were obtained from a DSC 1 STAR System (Mettler-Toledo) over a temperature range of 25–300 °C. Thermal gravimetric analysis (TGA) was analyzed on a TGA/DSC 1 STAR System (Mettler-Toledo) with a temperature range of 25–800 °C and a heating rate of 10 °C/min. Section morphology of



Scheme 1. Synthetic route of shape memory PAEK.

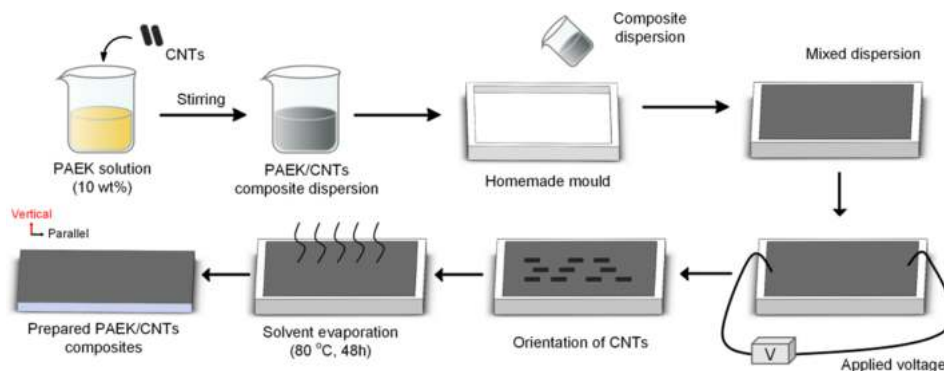


Fig. 1. Fabrication process of oriented CNTs/PAEK composites. (For interpretation of the references to colour in this figure legend, the reader is referred to the web version of this article.)

Table 1

Feed content of CNTs and applied voltages for CNTs orientation.

Sample: PAEK 10 V voltage	Content of CNTs			
	0 wt%	5 wt%	10 wt%	15 wt%
Sample: PAEK 10 wt% CNTs	Applied voltage for CNTs orientation			
	0 V	5 V	10 V	15 V

PAEK/CNTs composites on parallel and vertical current directions was observed using a scanning electron microscope (S-4300, Hitachi). Before testing, the samples were brittle fractured by liquid nitrogen and sputtered gold. Mechanical properties of PAEK/CNTs composites on parallel and vertical current directions were measured from a universal mechanical testing machine (SBA-10, Hake Keji). The samples were cut into the size of 30 mm × 10 mm. The gauge length was 20 mm and the loading rate of 4 mm/min. The testing results were averaged from 5 samples.

2.5. Shape memory test

The heat-triggered shape memory behaviors of PAEK/CNTs composites on parallel and vertical current directions were investigated through the “U” shape samples. The samples with the size of 10 mm × 30 mm were fixed into a “U” shape by the mould above the temperature of T_g . Then, they were cooled down quickly to room temperature for shape fixity. The samples were detached from the mould, and the angle was recorded (θ_0). Afterwards, the temperature was increased to $T_g + 10$ °C, and the shape recovery could be observed. The whole recovery process was recorded by a digital video camera. The recovery ratio (R_r) and fixity ratio (R_f) were calculated from the following formulas:

$$R_r = \frac{\theta(t) - \theta_0}{180 - \theta_0} \times 100$$

$$R_f = \frac{180 - \theta_0}{180} \times 100$$

where θ_0 is the deformation angle at time of 0 s, and $\theta(t)$ is at time of t s.

The electric-actuated shape memory behaviors of PAEK/CNTs composites on parallel and vertical current directions were investigated through the similar steps mentioned above. The fixity of temporary shape was the same, whereas the shape recovery was triggered by the electricity. The samples with fixed temporary shape were imposed with different triggering voltages for shape recovery. The whole process was recorded, and R_r , R_f could be calculated. In addition, the conductivity of PAEK/CNTs composites was measured by a RT-70V/RG-7C four-point probe (Napson Corp).

3. Results and discussion

3.1. Characterization

The chemical structures of synthesized PAEK could be characterized by ^1H NMR analysis, shown in Fig. 2a. The chemical shifts at 7.09 ppm, 7.26 ppm, and 7.80 ppm, were corresponded to the protons of 1, 2, and 3 [31]. FTIR spectra is showed in Fig. 2b. For pure PAEK, the peak at 1656 cm^{-1} was attributed to the stretching vibration of aryl carbonyl groups, and the peak at 1239 cm^{-1} was concerned with the characteristic peak of aryl ether groups. Meanwhile, there was not any differences of peaks position after the addition of CNTs, indicating the physical blends between PAEK and CNTs. In addition, after incorporating CNTs, the transmittance of composites decreased, due to intrinsic dark-color feature of CNTs.

WAXD curves are showed in Figure S1. Pure PAEK showed characteristic diffraction peak, which became broader after the addition of CNTs, indicating that the integration of CNTs destructed the crystalline structure of PAEK. Nevertheless, while the CNTs content reached up to 15 wt%, the diffraction peak got sharp, which could be attributed to the aggregation of CNTs in PAEK matrix. Comparing with the relative homogeneous dispersion of CNTs in PAEK matrix, the aggregation of CNTs didn't cause the destruction of crystalline of PAEK.

DSC and TGA curves are showed in Fig. 3. In Fig. 3a, the glass transition temperature (T_g) of the composites was 168.8 °C, 169.9 °C, 171.6 °C, and 171.3 °C, corresponding to the CNTs content of 0 wt%, 5 wt%, 10 wt%, and 15 wt%, respectively. In Fig. 3b, the first degradation stage occurred at around 130 °C, which was concerned with the removal of nonvolatile solvent and absorbed water. The degradation of PAEK main chains occurred at around 495 °C, which postponed slightly after the addition of CNTs. When the temperature reached up to 800 °C, as the increasing of CNTs content, the residual mass of composites increased gradually from 31.2%, to 34.9%, 50.1%, and 52.2%, corresponding to the CNTs content of 0 wt%, 5 wt%, 10 wt%, and 15 wt%, respectively.

The microstructural characteristics of PAEK/CNTs composites on parallel to current direction with diverse CNTs contents and different applied voltages are showed in Fig. 4. It could be observed that as the increasing of CNTs content from 5 wt% to 15 wt%, the CNTs in matrix became dense and aggregated. For the samples with 10 wt% CNTs, as the increasing of applied voltage, the oriented dispersion of CNTs became more obvious and almost all the CNTs were rearranged in the same direction after treatment at applied voltage of 15 V.

The parallel and vertical morphologies of PAEK/10 wt% CNTs composites treated with different applied voltages are showed in Fig. 5. When increasing applied voltage to 15 V, the radial alignment of CNTs became mostly significant. In parallel direction, the CNTs in images were almost rearranged to a direction. The sectional images show that, as the increasing of applied voltage, the arrangement of CNTs became dense in vertical direction, which further reflected the orientation of

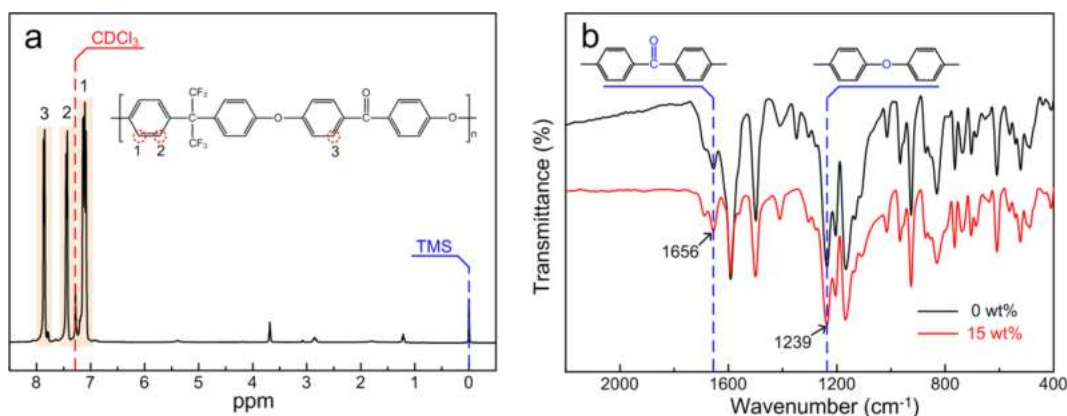


Fig. 2. Characterization of synthesized PAEK and PAEK/CNTs composites: a ^1H NMR spectra; b FTIR spectra (CNTs content of 0 wt% and 15 wt%). (For interpretation of the references to colour in this figure legend, the reader is referred to the web version of this article.)

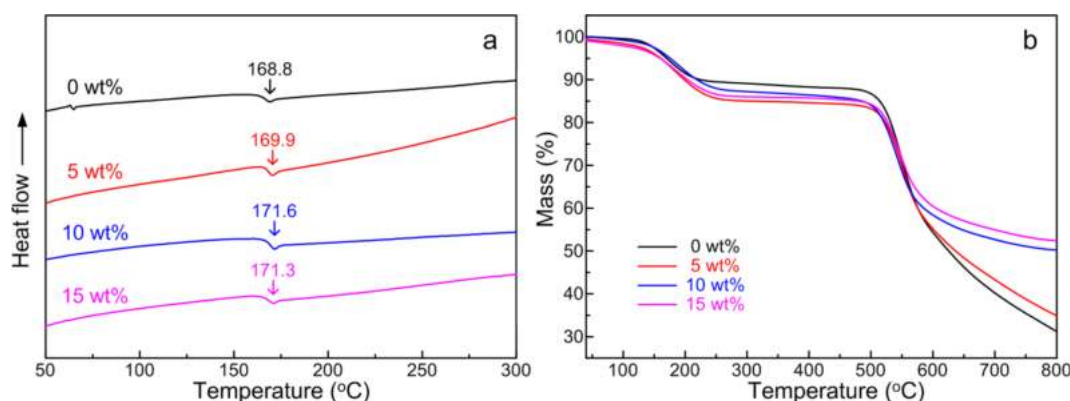


Fig. 3. DSC (a) and TGA (b) curves of PAEK/CNTs composites with different CNTs content (0 wt%, 5 wt%, 10 wt%, and 15 wt%). (For interpretation of the references to colour in this figure legend, the reader is referred to the web version of this article.)

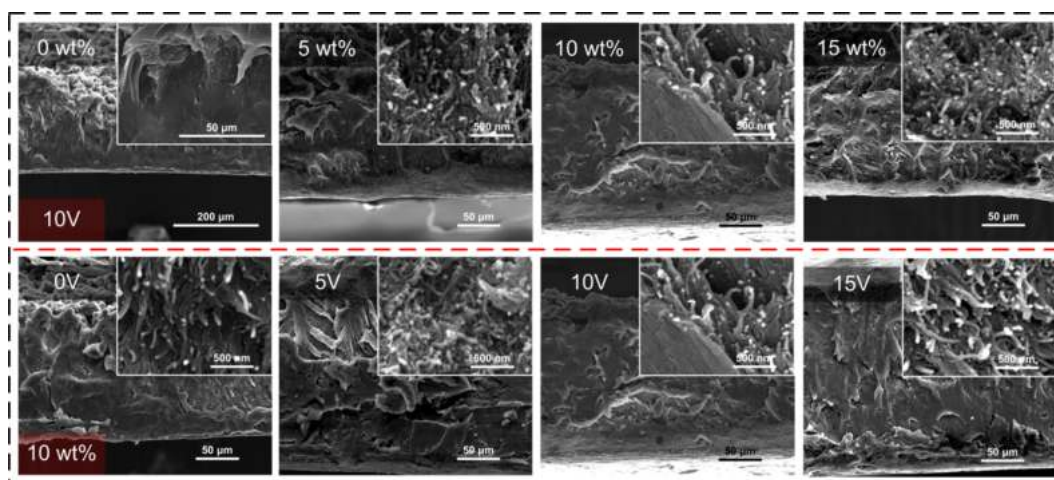


Fig. 4. SEM images of PAEK/CNTs composites on parallel direction: (upper row) samples with different content of CNTs (0 wt%, 5 wt%, 10 wt%, and 15 wt%) treated by the applied voltage of 10 V, and (lower row) samples of 10 wt% CNTs treated by different applied voltage (0 V, 5 V, 10 V, and 15 V). (For interpretation of the references to colour in this figure legend, the reader is referred to the web version of this article.)

CNTs.

3.2. Mechanical performances

Static tensile test results of PAEK/CNTs composites on parallel and vertical directions are showed in Fig. 6 (a-f: the samples on parallel

direction were employed for testing). Fig. 6a shows the stress-strain patterns of the composites with various CNTs content. Pure PAEK sample exhibited the yield stage during the tensile process, and with the increasing of CNTs content, the yield stage occurred earlier, at the strain of 5.43%, 4.48%, and 4.19% corresponding to the CNTs content of 0 wt%, 5 wt%, and 10 wt%, respectively. When the content of CNTs was 15

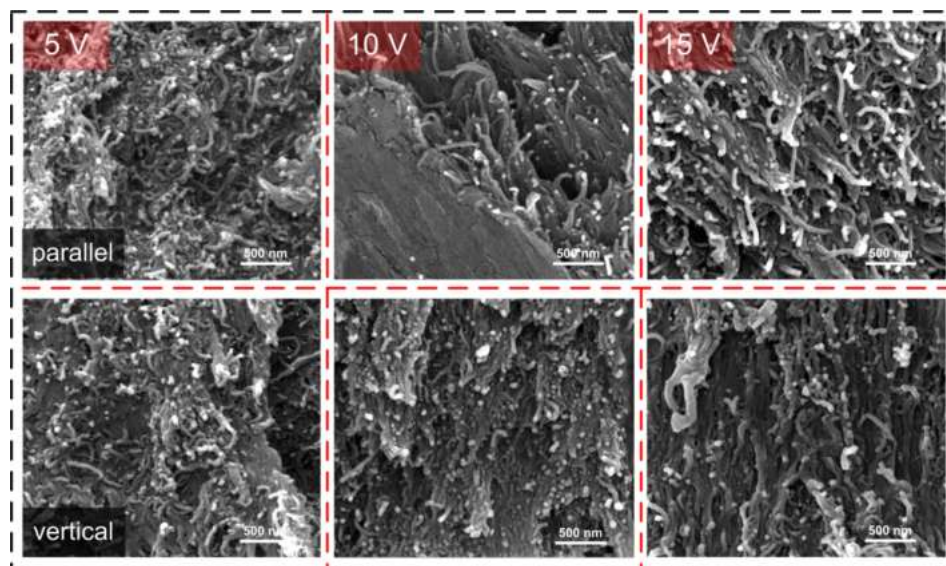


Fig. 5. SEM images of PAEK/CNTs composites on parallel direction and vertical direction with 10 wt% CNTs upon different applied voltages (5 V, 10 V, and 15 V). (For interpretation of the references to colour in this figure legend, the reader is referred to the web version of this article.)

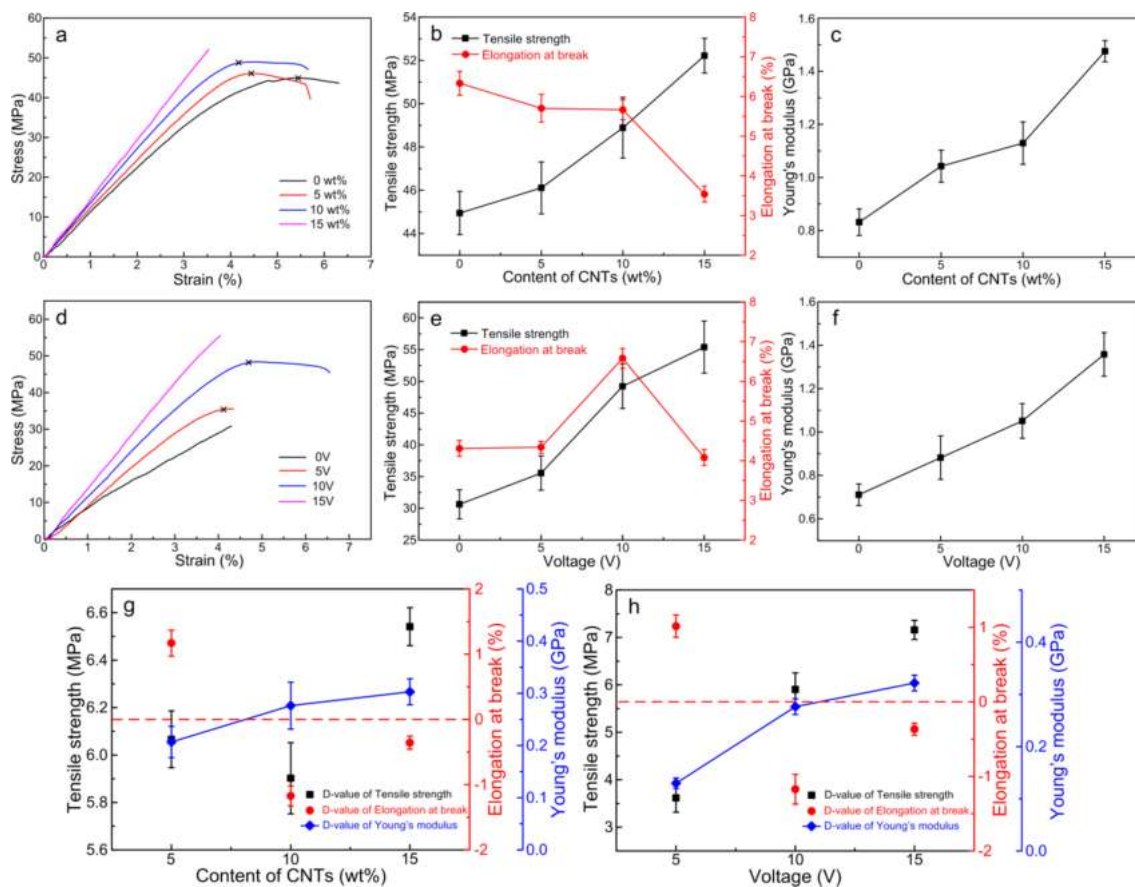


Fig. 6. Static tensile test results of PAEK/CNTs composites on parallel direction and vertical direction: (a) Stress–strain curves of the composites upon voltage of 10 V; (b) Tensile strength and elongation at break of the composites upon voltage of 10 V; (c) Young's modulus of the composites upon voltage of 10 V; (d) Stress–strain curves of the composites with CNTs content of 10 wt%; (e) Tensile strength and elongation at break of the composites with CNTs content of 10 wt%; (f) Young's modulus of the composites with CNTs content of 10 wt%; (g) D-value of mechanical properties of the composites upon the voltage of 10 V between parallel and vertical directions; (h) D-value of mechanical properties of the composites with CNTs content of 10 wt% between parallel and vertical directions (a–f: the samples on parallel direction were employed for testing). (For interpretation of the references to colour in this figure legend, the reader is referred to the web version of this article.)

wt%, the fracture mode changed to brittle fracture, and there was not the occurrence of yield stage. Fig. 6b reflected the effect of CNTs content on tensile strength and elongation at break. As the increasing of CNTs content from 0 wt%, 5 wt%, 10 wt%, and 15 wt%, the corresponding tensile strength gradually increased, from 44.95 MPa to 46.11 MPa, 48.89 MPa, and 52.22 MPa, respectively. Meanwhile, the elongation at break decreased from 6.33% to 5.70%, 5.67%, and 3.54%, respectively. The phenomenon could be attributed to that the enhanced stiffness of CNTs increased the strength, whereas weakened the toughness of composites. As a result, with the increasing of CNTs content, the tensile strength increased, and the elongation at break decreased. The changing trend of Young's modulus is showed in Fig. 6c. As the increasing of CNTs content, Young's modulus increased gradually, from 0.83 GPa to 1.04 GPa, 1.13 GPa, and 1.48 GPa, corresponding to CNTs content of 0 wt%, 5 wt%, 10 wt%, and 15 wt%, respectively. It also should be concerned with the introduction of high stiff CNTs, as mentioned above.

Fig. 6d shows the effect of applied voltage on stress-strain behaviors of the composites. It could be observed that, without applied voltage, the sample was brittle fracture because of the randomly dispersed CNTs in PAEK matrix. When applying the voltage (5 V and 10 V), CNTs were rearranged to become obediently dispersed in matrix, promoting the roughness of composites. As a result, yield stage occurred during the tensile process. When the applied voltage was 15 V, the orientation of CNTs was adequate, which tightly placed in matrix (observed in SEM images). Due to the intrinsic stiffness, composites exhibited decreased toughness, and the fracture mode became brittle fracture. The effect of applied voltage on tensile strength and elongation at break is showed in Fig. 6e. With the increasing of applied voltage, tensile strength gradually increased, from 30.63 MPa to 35.55 MPa, 49.23 MPa, and 55.39 MPa, corresponding to the voltage of 0 V, 5 V, 10 V, and 15 V, respectively. While applied voltage was 0 V and 5 V, elongation at break had almost no change, of 4.31% and 4.34%, respectively. When the applied voltage was 10 V, the toughness of composites was significantly reinforced, and the elongation at break was 6.58%, which could be concerned with the pull out effect [32,33] of CNTs in PAEK matrix during the stretching process, depicted in Figure S2. Nevertheless, when applied voltage increased to 15 V, tight placement of CNTs in matrix was detrimental to the toughness, and as a result, elongation at break was 4.08%. Fig. 6f shows the effect of applied voltage on Young's modulus. With the increasing of applied voltage, oriented dispersion of CNTs in matrix reinforced Young's modulus, from 0.71 GPa to 0.88 GPa, 1.05 GPa, and 1.36 GPa, corresponding to the voltage of 0 V, 5 V, 10 V, and 15 V, respectively.

Difference value (D-value), in this paper, was defined as the value of which on parallel direction subtracted the value on vertical direction. D-value of mechanical properties of the composites upon the voltage of 10 V are showed in Fig. 6g. As the increasing of CNTs content, D-value of tensile strength was almost increased, of 6.07 MPa, 5.90 MPa, and 6.54 MPa, corresponding to the CNTs content of 5 wt%, 10 wt%, and 15 wt%, respectively. As for elongation at break, D-value was 1.17%, -1.17%, and -0.36%, corresponding to the CNTs content of 5 wt%, 10 wt%, and 15 wt%, respectively. As the increasing of CNTs, D-value of Young's modulus gradually increased, from 0.21 GPa to 0.28 GPa, and 0.30 GPa, corresponding to CNTs content of 5 wt%, 10 wt%, and 15 wt%, respectively. The increasing of CNTs content quantitatively improved the orientation extend of CNTs, reinforcing the Young's modulus. D-value of mechanical properties of the composites with CNTs content of 10 wt% are showed in Fig. 6h. With the increasing of applied voltage, D-value of tensile strength gradually increased from 3.62 MPa, 5.90 MPa, and 7.16 MPa corresponding to the voltage of 5 V, 10 V, and 15 V, respectively. Increasing the applied voltage, the orientation extent of CNTs improved, conducive to the tensile strength. D-value of elongation at break was 1.02%, -1.17%, and -0.37%, corresponding to the voltage of 5 V, 10 V, and 15 V, respectively. As for Young's modulus, D-value increased gradually as the increasing of applied voltage, from 0.13 GPa to 0.28 GPa, and 0.32 GPa, corresponding to the voltage of 5 V, 10 V,

and 15 V, respectively.

3.3. Heat-actuated shape memory behaviors

Heat-actuated shape memory behaviors of PAEK/CNTs composites were investigated and showed in Fig. 7 (a-c: the samples on parallel direction were employed for testing). The whole shape recovery process of the composites with CNTs content of 10 wt% upon the applied voltage of 10 V at 181 °C ($T_g + 10$ °C) is showed in Fig. 7a. The whole shape recovery process could finish within 12 s as the sample recovered approximately to the permanent shape of "bar" shape from the temporary shape of "U" shape (The whole shape recovery process was recorded in Video S1). Fig. 7b reflected the effect of CNTs content on recovery ratio of the composites. Synthesized PAEK sample exhibited the excellent recovery behaviors, whose recovery ratio of 96.5%. As the addition of CNTs, the recovery ratio of the composites decreased, of 93.7% and 94.9%, corresponding to CNTs content of 5 wt% and 10 wt%, respectively. It could be attributed to that the integration of tubular and stiff CNTs in PAEK matrix was detrimental to the movement of molecular chains above triggering temperature, which decreased the recovery ratio. When the CNTs content increased to 15 wt%, recovery ratio decreased to 78.2%, which could be concerned with that the dense dispersion of CNTs in matrix seriously hindered the movement of molecular chains of PAEK. Fig. 7c reflected the effect of applied voltage on recovery ratio of the composites. The recovery ratio of the composites with CNTs content of 10 wt% without applied voltage was 93.2%. As the increasing of applied voltage, the recovery ratio of increased gradually, of 94.2%, 94.9%, and 98.7%, corresponding to the voltage of 5 V, 10 V, and 15 V, respectively. The orientation of CNTs in matrix occurred by applied voltage, and the orientation extent became higher as the increasing of the voltage. Due to the intrinsic thermal conductivity of CNTs [34], the radially aligned CNTs array formed efficient thermal conduction path in PAEK matrix, conducive to the heat transmission in the composites. Besides, comparing with random dispersion of CNTs in matrix, obediently oriented CNTs were not so detrimental to the movement of molecular chains along with the macroscopic movement direction. Fig. 7d shows the recovery ratio of the composites with CNTs content of 10 wt% upon different applied voltage (5 V, 10 V, and 15 V) on parallel and vertical directions. While the CNTs content was 10 wt%, the recovery ratio of obtained samples were above 93%, whatever the composites on parallel direction or vertical direction, indicating to the good shape recovery capability. It could be observed that the recovery ratio of the composites on parallel direction was slightly higher than it on vertical direction, and the D-value became larger with the increasing of applied voltage (of 0.4%, 1.3%, and 3.2%, corresponding to the voltage of 5 V, 10 V, and 15 V, respectively). It might be concerned with the fabrication and enhancement of thermal conduction path. Fig. 7e shows the fixity ratio of the composites with diverse content of CNTs, upon different voltage, on parallel and vertical directions. It could be observed that the fixity ratio of all the samples were over 98%, indicating the excellent shape fixity capability. With increasing of the CNTs contents and the applied voltage, the fixity ratio increased. The oriented and dense dispersion of CNTs in PAEK matrix expanded the rigid segments in the composites, promoting the shape fixity. Besides, the fixity ratio of the composites on parallel direction always slightly higher than the corresponding sample on vertical direction.

3.4. Electric-actuated shape memory behaviors

The electric-actuated shape memory behaviors of PAEK/CNTs composites were investigated and illustrated in Fig. 8 (a-d: the samples on parallel direction were employed for testing, and the imposed triggering voltage was 40 V). Fig. 8a shows the whole shape recovery process of the composites with CNTs content of 10 wt% upon applied voltage of 10 V. The original shape could be recovered within 10 s, which exhibited the electric-actuated rapid recovery capability. Thermal infrared images

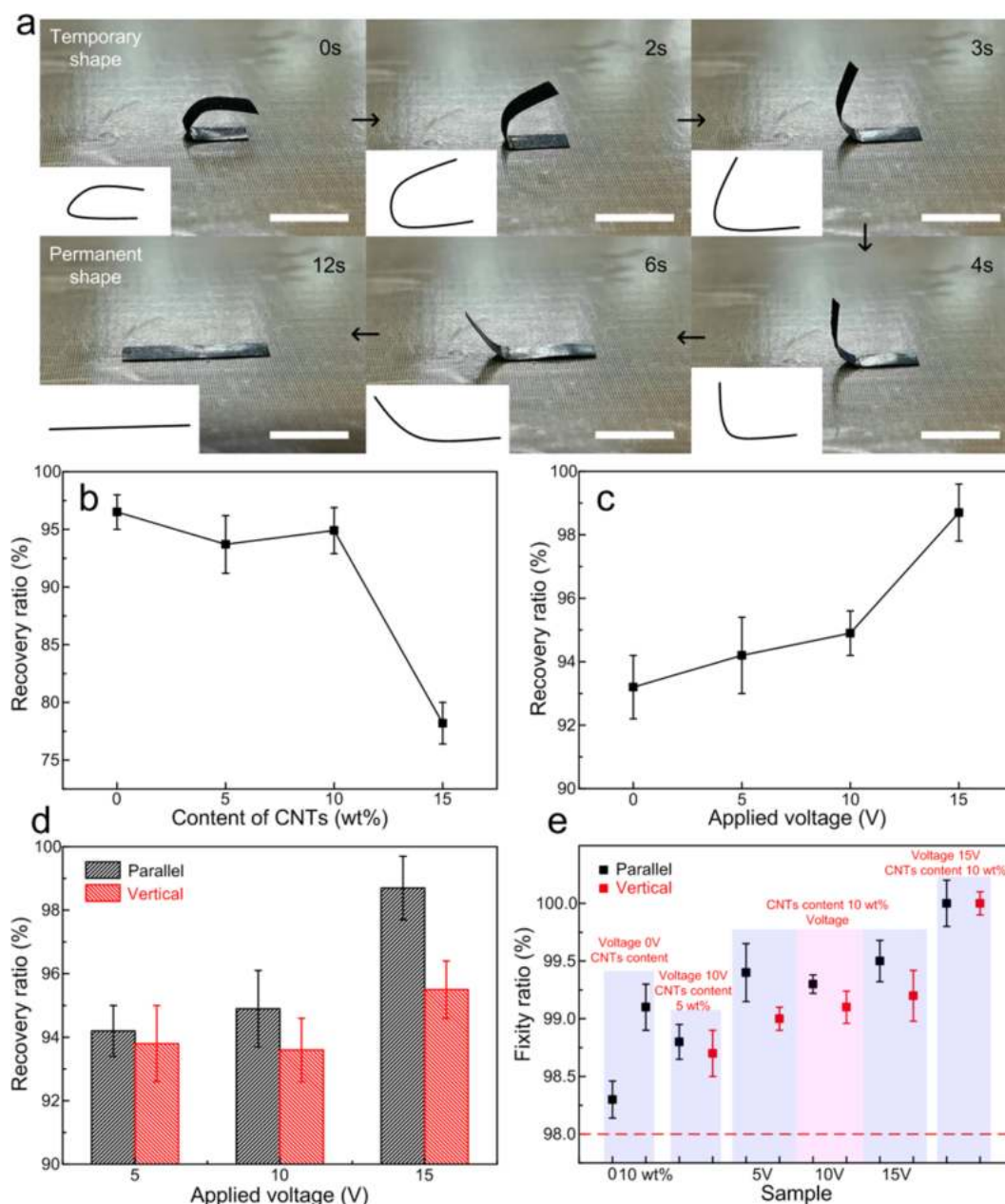


Fig. 7. Heat-actuated shape memory behaviors of PAEK/CNTs composites: (a) The whole shape recovery process of the composites with CNTs content of 10 wt% upon the voltage of 10 V at 181 °C ($T_g + 10$ °C); (b) Recovery ratio of the composites upon the voltage of 10 V with different content of CNTs (0 wt%, 5 wt%, 10 wt%, and 15 wt%); (c) Recovery ratio of the composites with CNTs content of 10 wt% upon different applied voltage (0 V, 5 V, 10 V, and 15 V); (d) Recovery ratio of the composites with CNTs content of 10 wt% upon different applied voltage (5 V, 10 V, and 15 V) on parallel and vertical directions; (e) Fixity ratio of the composites with diverse content of CNTs, upon different voltage, on parallel and vertical directions (a-c: the samples on parallel direction were employed for testing, in addition that untagged scale bars of 1 cm). (For interpretation of the references to colour in this figure legend, the reader is referred to the web version of this article.)

were captured for the monitoring of the temperature variation caused by the electrothermal effect of CNTs, depicted in Fig. 8b. Along with constant triggering voltage, the temperature increased rapidly, which finally reached up to 107.1 °C as the achievement of the recovery process. Fig. 8c shows the recovery ratio of composites with diverse content of CNTs. As the increasing of CNTs content, the recovery ratio increased gradually, from 82.2% to 93.2%, and 94.2%, corresponding to the CNTs content of 5 wt%, 10 wt%, and 15 wt%, respectively. In these tests, the samples on parallel direction were employed, and the recovery ratio of samples on vertical direction was lower than the corresponding samples on parallel direction, shown in Fig. 8e. Meanwhile, the composites with CNTs content of 5 wt% on vertical direction could not achieve the shape recovery upon the triggering voltage of 40 V, which indicated the

significance of the orientation of CNTs in PAEK matrix by applied voltage. The recovery ratio of composites with diverse applied voltage is showed in Fig. 8d. As the increasing of applied voltage, the recovery ratio of the composites with CNTs content of 10 wt% increased gradually, from 82.4%, to 85.7%, 93.2%, and 94.2%, corresponding to the voltage of 0 V, 5 V, 10 V, and 15 V, respectively. With the increasing of applied voltage, the orientation extent of CNTs improved, which conducive to the current path and promoting to the shape recovery. Fig. 8e shows the recovery ratio of the composites upon different applied voltage on parallel and vertical directions. The recovery ratio of the composites on parallel direction was slightly higher than that of the samples on vertical direction, which could be closely related to the enhancement of conductive path. Due to the shape fixity of the

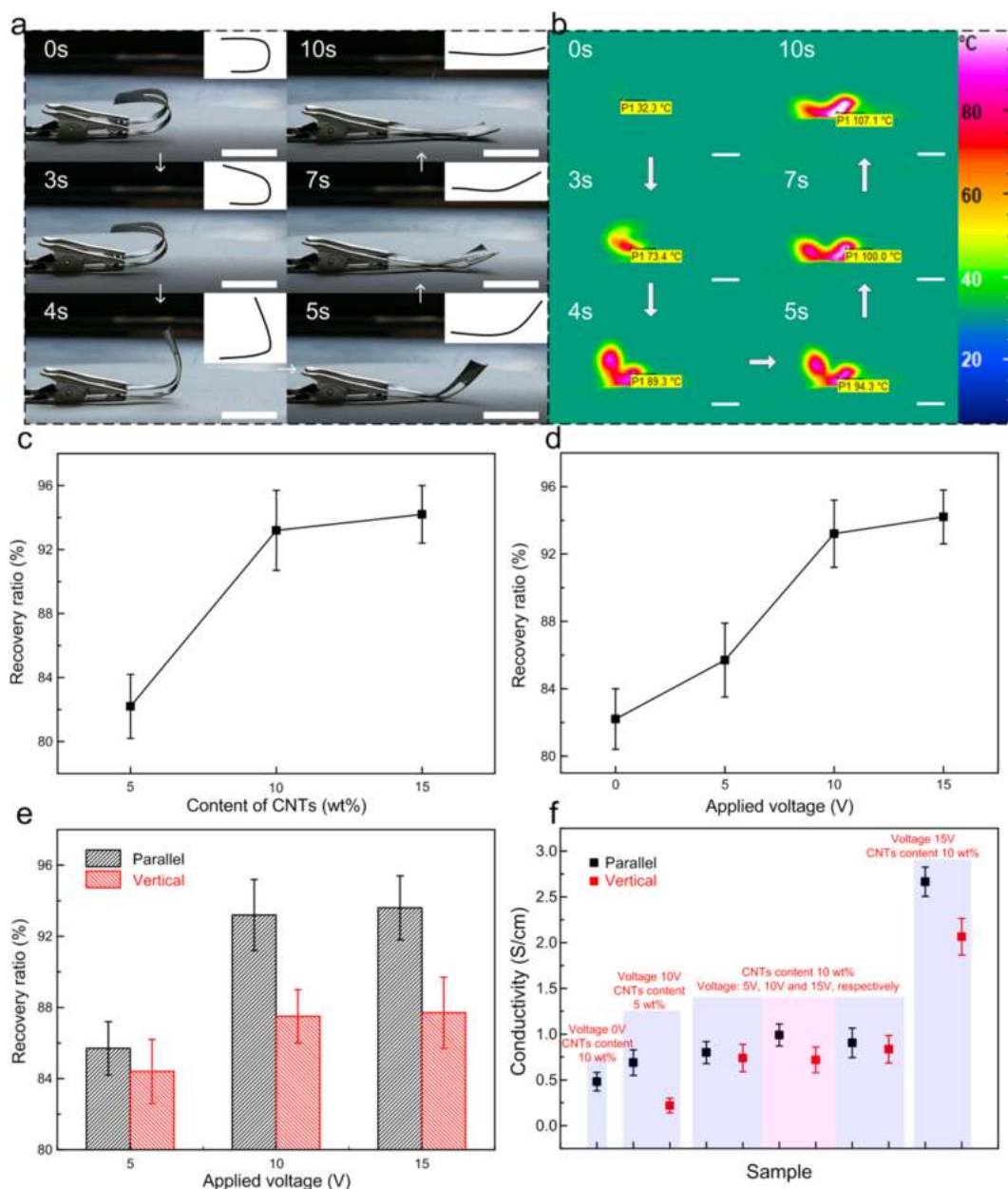


Fig. 8. Electric-actuated shape memory behaviors of PAEK/CNTs composites: (a) The whole shape recovery process of the composites with CNTs content of 10 wt% and applied voltage of 10 V at the triggering voltage of 40 V; (b) Thermal infrared images of the whole shape recovery process; (c) Recovery ratio of the composites with different content of CNTs (5 wt%, 10 wt%, and 15 wt%) upon applied voltage of 10 V; (d) Recovery ratio of the composites with CNTs content of 10 wt% upon different applied voltage (0 V, 5 V, 10 V, and 15 V); (e) Recovery ratio of the composites with CNTs content of 10 wt% upon different applied voltage (5 V, 10 V, and 15 V) on parallel and vertical directions; (f) Conductivity of the composites with diverse content of CNTs, upon different voltage, on parallel and vertical directions (a-e: the samples on parallel direction were employed for testing, and the imposed triggering voltage was 40 V, in addition that untagged scale bars of 1 cm). (For interpretation of the references to colour in this figure legend, the reader is referred to the web version of this article.)

composites triggered by electric was the same with them triggered by heat, it was not repeatedly illustrated. Fig. 8f shows the conductivity of the composites with diverse CNTs contents on parallel and vertical directions. Significantly, the conductivity of the composites on parallel direction was always slightly higher than the corresponding sample on vertical direction. All the samples except for the sample with 5 wt% content of CNTs on vertical direction could realize the shape recovery. The electrothermal effect of 5 wt% CNTs with the lowest conductivity of 0.219 S/cm could not provide the sufficient thermal power to trigger the shape recovery. When the content of CNTs was 15 wt%, the conductivity increased significantly, and the triggering voltage decreased from 40 V to 30 V. The orientation of CNTs was instrumental in the construction and enhancement of current path, and as a result, the conductivity

increased.

3.5. Rapid heat- and electric-response

Upon the applied voltage, CNTs were significantly oriented in PAEK matrix consistent with the current direction. With the increasing of CNTs content, continuous radially aligned CNTs constructed an efficient conductive path, conducive to the thermal conductivity and electric conductivity, as depicted in Fig. 9a. Thereby, heat- and electric-triggered shape memory behaviors could be strengthened through the construction of conductive path. Fig. 9b shows the heat-actuated shape recovery behaviors of the PAEK/CNTs composites with the same CNTs content and applied voltage, except for the current direction. The

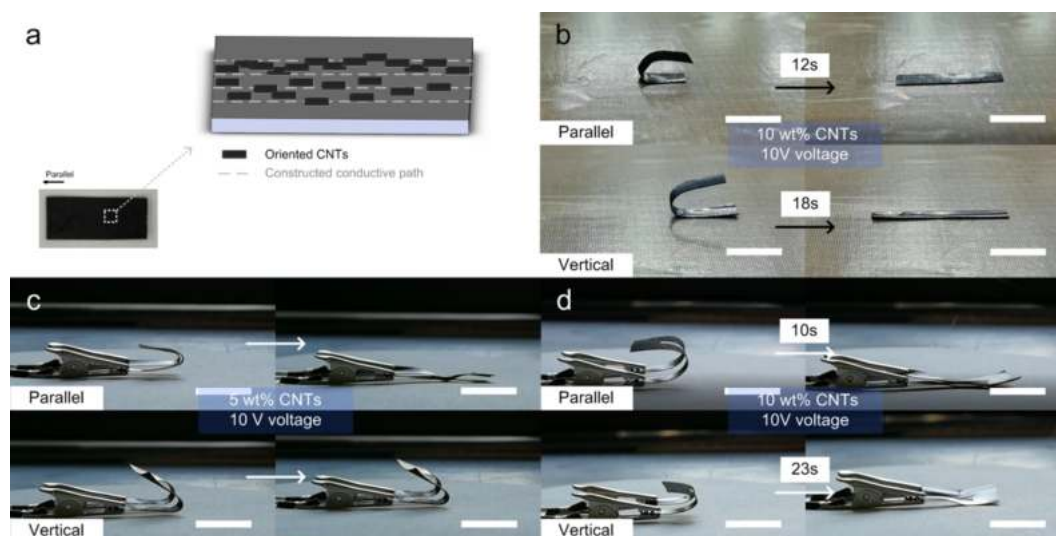


Fig. 9. Efficient heat/electric dual triggered shape memory behaviors: (a) Construction of conductive path of oriented CNTs; (b) Rapid heat-triggered shape recovery behaviors; (c) Low triggering voltage; (d) Efficient electric-triggered shape recovery behaviors (triggering temperature of $181\text{ }^{\circ}\text{C}$ ($T_g + 10\text{ }^{\circ}\text{C}$), and imposed triggering voltage of 40 V , in addition that untagged scale bars of 1 cm). (For interpretation of the references to colour in this figure legend, the reader is referred to the web version of this article.)

composite on parallel direction exhibited the more rapid shape recovery pace (within 12 s) than it on vertical direction (within 18 s), which were due to the internal constructed conductive path. In Fig. 9c, when the CNTs content was $5\text{ wt}\%$, the composite on parallel direction could recover to its original shape actuated by the electricity, but on vertical direction it could not be actuated by electric power. In Fig. 9d, the composite on parallel direction exhibited more efficient shape recovery than it on vertical direction. These radially aligned CNTs/PAEK composite actuators containing efficient heat/electric dual triggered shape memory effect exhibited exciting application prospects.

3.6. Voltage actuators

Based on the investigations above, we employed aligned CNTs/PAEK composites with $15\text{ wt}\%$ CNTs as the voltage actuators, due to the excellent mechanical performances and durability. Besides, comparing with the PAEK/CNTs on vertical direction, aligned CNTs/PAEK composites exhibited rapid electric-response speed and extended applied voltage ranges, which imparted the voltage actuators the enhanced

sensitivity and large actuating range. Initially, we investigated the recovered angles of the composite actuators at the different voltage, shown in Fig. 10. The range of applied voltage was from 8 V to 50 V , which was attributed to that the voltage below 8 V could not triggered the shape recovery of actuators, in addition that the recovery angle and speed did not exhibit difference while the voltage over 50 V . It could be obtained that the recovered angles gradually increased when the voltage was lower than 20 V . In this stage, the treated time was 300 s , in order to obtain the completed recovered angles. While the voltage was from 20 V to 25 V , the actuators almost finished the shape recovery within 110 s , and the recovered angles increased up to around 155° . Subsequently, continually increased the voltage, the recovered angles almost kept stability and the recovered time decreased.

According to the diverse recovered angles and time, shown in Fig. 10, we designed the two kinds of voltage actuators catering to different voltages. In Fig. 11a, we used the recovered angles of voltage actuators to measure the actuating actions. Different applied voltage could trigger the actuator to deform to the different angles, and as the increasing of voltage, the recovered angles increased. It was visual to obtain the actuating actions through the recovered angles of the actuators. In addition, in this mode, the applied range of actuators was from 8 V to 19 V . While the applied voltage was over 20 V , we could use the recovered time of voltage actuators to measure the actuating actions, shown in Fig. 11b. When the testing voltage was $20\text{--}22\text{ V}$, the recovered time was almost 110 s , and when it increased to 25 V , the recovered time was decreased to 35 s . Afterwards, the gradual decreasing of recovered time reflected the increasing of testing voltage. We could obtain the testing voltage value in accordance with the recovered time of the sensors. In this time-mode, the testing range of sensors was from 20 V to 50 V . The angle and time mode of voltage sensors was employed to visually measure the testing voltage, which imparted the wide using potential in fields of electronic devices.

The durability and stability were significant for sensors, and we conducted the continuous voltage actuating testing to measure the durability of aligned CNTs/PAEK composites actuators, as shown in Fig. 12. For angle-mode, it could be obtained that the recovered angles of actuators almost kept stable during the cyclic sensing test. For time mode, we could observe that the actuators finished the shape recovery behaviors within 5 s during the cyclic sensing test. The stability of angle-mode and time-mode indicated the great durability of the composite actuators and convinced the regular operation.

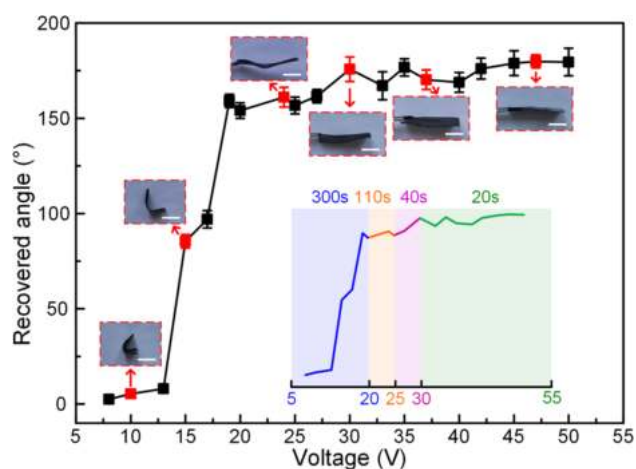


Fig. 10. Recovered angles of aligned CNTs/PAEK composite actuators upon the voltage of the range from 8 V to 50 V (scale bars of 1 cm). (For interpretation of the references to colour in this figure legend, the reader is referred to the web version of this article.)

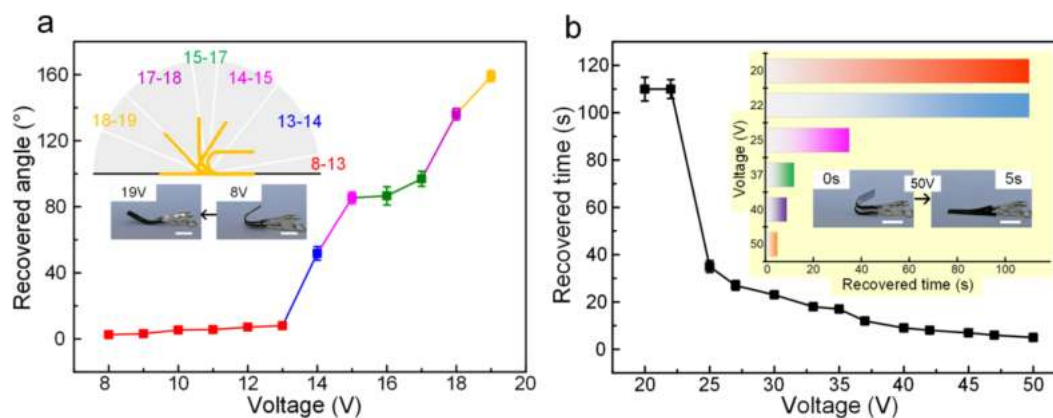


Fig. 11. (a) The operation mechanism of voltage actuators-angle mode at the applied voltage with the range of 8–19 V; (b) The operation mechanism of voltage actuators-time mode at the applied voltage with the range of 20–50 V (scale bars of 1 cm). (For interpretation of the references to colour in this figure legend, the reader is referred to the web version of this article.)

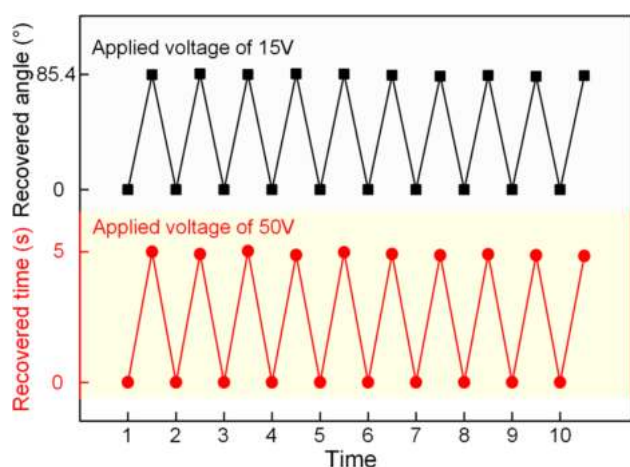


Fig. 12. Continuous voltage actuating behaviors of aligned CNTs/PAEK composite actuators. (For interpretation of the references to colour in this figure legend, the reader is referred to the web version of this article.)

4. Conclusions

In summary, we synthesized the shape memory PAEK via nucleophilic substitution reaction, and fabricated PAEK/CNTs composites with oriented CNTs conductive paths via an electro-mixed fusion method. The composites exhibited the excellent thermal stability due to the intrinsic properties of PAEK and the incorporation of CNTs. The dispersion and orientation of CNTs in PAEK matrix were greatly affected by CNTs content, applied voltage, and current directions. Mechanical performances of composites were reinforced remarkably via the integration and orientation of CNTs in PAEK matrix. As the increasing of CNTs content, the tensile strength and Young's modulus increased gradually, whereas the elongation at break decreased. As the increasing of applied voltage, the tensile strength and Young's modulus increased. Meanwhile, the strength and modulus of composites on parallel direction were higher than that on vertical direction, concerning with the continuous and oriented arrangement of CNTs in PAEK matrix. Besides, as the increasing of CNTs content and applied voltage, the reinforcement of strength and modulus on parallel direction was more significant.

The PAEK/CNTs composites exhibited excellent heat/electric dual actuated shape memory behaviors. As for heat-actuated SME, as the increasing of CNTs content, the recovery ratio decreased. Nevertheless, it gradually increased with the increasing of applied voltage, which was attributed to the construction of thermal conductive path by continuous

oriented CNTs. Besides, the recovery ratio of composites on parallel direction was almost higher than that on vertical direction, which could be concerned with the same reason. In addition, composites exhibited excellent fixity ratio which were all over 98%. As for electric-actuated SME, as the increasing of CNTs content, the recovery ratio increased due to the electrothermal effect of CNTs. As the increasing of applied voltage, the recovery ratio increased because of the construction of conductive path. The shape recovery ratio of composites on parallel direction was always higher than those on vertical direction, which could be related to the enhancement of conductive path. Meanwhile, the conductivity of the composites on parallel direction was always slightly higher than the corresponding sample on vertical direction. Upon the applied voltage, radially aligned CNTs constructed the conductive path in PAEK matrix, which was instrumental to the thermal conductivity and electrical conductivity. Therefore, rapidly efficient heat/electric dual actuated shape memory behaviors were achieved at low triggering voltage.

In addition, we employed aligned CNTs/PAEK composites with 15 wt % CNTs as the voltage actuators due to the excellent mechanical performances, durability, rapid electric-response speed and wide working voltage ranges. We designed the two kinds of voltage actuators (angle-mode and time-mode) to achieve the measurement of actuating actions (range from 8 V to 50 V). For angle-mode, we could measure the actuating actions at the range of 8–19 V, and the time-mode of voltage actuators could be used while the applied voltage was 20–50 V. These efficient composite voltage actuators exhibited the excellent stability and durability in continuous voltage actuating testing. We proposed a facile fabrication of an efficient radially aligned CNTs/PAEK heat/electric dual triggered shape memory composite voltage actuators which developed the exciting potential in smart actuators and electronic devices.

CRediT authorship contribution statement

Shuai Yang: Conceptualization, Methodology, Data curation, Writing – original draft, Writing – review & editing. **Yang He:** Supervision, Data curation, Conceptualization, Methodology, Writing – review & editing. **Yanju Liu:** . **Jinsong Leng:** Conceptualization, Supervision, Resources, Funding acquisition, Project administration, Writing – review & editing.

Declaration of Competing Interest

The authors declare that they have no known competing financial interests or personal relationships that could have appeared to influence the work reported in this paper.

Acknowledgements

This work is supported by the National Natural Science Foundation of China (Grant No. 11632005), and Heilongjiang Touyan Innovation Team Program.

Appendix A. Supplementary material

Supplementary data to this article can be found online at <https://doi.org/10.1016/j.compositesa.2022.106940>.

References

- Jang D, Farooq SZ, Yoon HN, Khalid HR. Design of a highly flexible and sensitive multi-functional polymeric sensor incorporating CNTs and carbonyl iron powder. *Compos Sci Tech* 2021;207:108725. <https://doi.org/10.1016/j.compscitech.2021.108725>.
- He Y, Wu D, Zhou M, Zheng Y, Wang T, Lu C, et al. Wearable strain sensors based on a porous polydimethylsiloxane hybrid with carbon nanotubes and graphene. *ACS Appl Mater Inter* 2021;13(13):15572–83. <https://doi.org/10.1021/acsami.0c22823>.
- Worch JC, Weems AC, Yu J, Arno MC, Wilks TR, Huckstepp RTR, et al. Elastomeric polyamide biomaterials with stereochemically tuneable mechanical properties and shape memory. *Nat Commun* 2020;11(1). <https://doi.org/10.1038/s41467-020-16945-8>.
- Sachyani Keneth E, Scalet G, Layani M, Tibi G, Degani A, Auricchio F, et al. Pre-programmed tri-layer electro-thermal actuators composed of shape memory polymer and carbon nanotubes. *Soft Robot* 2020;7(2):123–9. <https://doi.org/10.1089/soro.2018.0159>.
- Sachyani Keneth E, Lieberman R, Rednor M, Scalet G, Auricchio F, Magdassi S. Multi-material 3D printed shape memory polymer with tunable melting and glass transition temperature activated by heat or light. *Polymers* 2020;12(3):710. <https://doi.org/10.3390/polym12030710>.
- Liu Y, Xu K, Chang Q, Darabi MA, Lin B, Zhong W, et al. Highly flexible and resilient elastin hybrid cryogels with shape memory, injectability, conductivity, and magnetic responsive properties. *Adv Mater* 2016;28(35):7758–67. <https://doi.org/10.1002/adma.201601066>.
- Xiao R, Huang WM. Heating/solvent responsive shape-memory polymers for implant biomedical devices in minimally invasive surgery: current status and challenge. *Macromol Biosci* 2020;20(8):2000108. <https://doi.org/10.1002/mabi.v20.8.10.1002/mabi.202000108>.
- Wu M, Sukyai P, Lv D, Zhang F, Wang P, Liu C, et al. Water and humidity-induced shape memory cellulose nanopaper with quick response, excellent wet strength and folding resistance. *Chem Eng J* 2020;392:123673. <https://doi.org/10.1016/j.cej.2019.123673>.
- Koga T, Tomimori K, Higashi N. Transparent, high-strength, and shape memory hydrogels from thermo-responsive amino acid-derived vinyl polymer networks. *Macromol Rapid Comm* 2020;41(7):1900650. <https://doi.org/10.1002/marc.v41.7.10.1002/marc.201900650>.
- Li X, Liu W, Li Y, Lan W, Zhao D, Wu H, et al. Mechanically robust enzymatically degradable shape memory polyurethane urea with a rapid recovery response induced by NIR. *J Mater Chem B* 2020;8(23):5117–30. <https://doi.org/10.1039/D0TB00798F>.
- Yan K, Xu F, Wang C, Li Y, Chen Y, Li X, et al. A multifunctional metal-biopolymer coordinated double network hydrogel combined with multi-stimulus responsiveness, self-healing, shape memory and antibacterial properties. *Biomater Sci* 2020;8(11):3193–201. <https://doi.org/10.1039/D0BM00425A>.
- Ghosh T, Voit B, Karak N. Polystyrene/thermoplastic polyurethane interpenetrating network-based nanocomposite with high-speed, thermo-responsive shape memory behavior. *Polymer* 2020;200:122575. <https://doi.org/10.1016/j.polymer.2020.122575>.
- Chatterjee T, Dey P, Nando GB, Naskar K. Thermo-responsive shape memory polymer blends based on alpha olefin and ethylene propylene diene rubber. *Polymer* 2015;78:180–92. <https://doi.org/10.1016/j.polymer.2015.10.007>.
- Chen Y, Zhao X, Luo C, Shao Y, Yang MB, Yin B. A facile fabrication of shape memory polymer nanocomposites with fast light-response and self-healing performance. *Compos Part A* 2020;135:105931. <https://doi.org/10.1016/j.compositesa.2020.105931>.
- Kang H, Lai H, Cheng Z, Liu Y, Jiang L. Restoration of superwetting switching on TiO₂ coated shape memory polymer arrays. *Chem Eng J* 2020;394:124996. <https://doi.org/10.1016/j.cej.2020.124996>.
- Zeng C, Liu L, Bian W, Liu Y, Leng J. 4D printed electro-induced continuous carbon fiber reinforced shape memory polymer composites with excellent bending resistance. *Compos Part B* 2020;194:108034. <https://doi.org/10.1016/j.compositesb.2020.108034>.
- Zhang F, Xia Y, Liu Y, Leng J. Nano/microstructures of shape memory polymers: from materials to applications. *Nanoscale Horiz* 2020;5(8):1155–73. <https://doi.org/10.1039/D0NH00246A>.
- Liu Y, Zhang W, Zhang F, Leng J, Pei S, Wang L, et al. Microstructural design for enhanced shape memory behavior of 4D printed composites based on carbon nanotube/poly(lactic acid) filament. *Compos Sci Technol* 2019;181:107692. <https://doi.org/10.1016/j.compscitech.2019.107692>.
- Adeel M, Zhao B, Li L, Zheng S. Nanocomposites of poly(hydroxyurethane)s with multiwalled carbon nanotubes: synthesis, shape memory, and reprocessing properties. *ACS Appl Polym Mater* 2020;2(4):1711–21. <https://doi.org/10.1021/acsapm.0c00183>.
- Liu Y, Guo Y, Zhao J, Chen X, Zhang H, Hu G, et al. Carbon fiber reinforced shape memory epoxy composites with superior mechanical performances. *Compos Sci Technol* 2019;177:49–56. <https://doi.org/10.1016/j.compscitech.2019.04.014>.
- Lin C, Lv J, Li Y, Zhang F, Li J, Liu Y, et al. 4D-printed biodegradable and remotely controllable shape memory occlusion devices. *Adv Funct Mater* 2019;29(51):1906569. <https://doi.org/10.1002/adfm.v29.51.10.1002/adfm.201906569>.
- Li CH, Zuo JL. Self-healing polymers based on coordination bonds. *Adv Mater* 2019;32:1903762. <https://doi.org/10.1002/adma.201903762>.
- Xu Z, Ding C, Wei DW, Bao RY, Ke K, Liu Z, et al. Electro and light-active actuators based on reversible shape-memory polymer composites with segregated conductive networks. *ACS Appl Mater Inter* 2019;11(33):30332–40. <https://doi.org/10.1021/acsami.9b10386>.
- Zhang ZX, Wang WY, Yang JH, Zhang N, Huang T, Wang Y. Excellent electroactive shape memory performance of EVA/PCL/CNT blend composites with selectively localized CNTs. *J Phys Chem C* 2016;120(40):22793–802. <https://doi.org/10.1021/acs.jpcc.6b06345>.
- Ren D, Chen Y, Yang S, Li H, Rehman HU, Liu H. Fast and efficient electric-triggered self-healing shape memory of CNTs@rGO enhanced PCLPLA copolymer. *Macromol Chem Phys* 2019;220(21):1900281. <https://doi.org/10.1002/macp.201900281>.
- Luo H, Li Z, Yi G, Zu X, Wang H, Huang H, et al. Multi-stimuli responsive carbon nanotube-shape memory polymeric composites. *Mater Lett* 2014;137:385–8. <https://doi.org/10.1016/j.matlet.2014.09.054>.
- Lin L, Zhou Q, Li M. A thermally and electrically shape memory polymer prepared by a novel electro-mixed fusion preparation method. *Mater Lett* 2019;256:126574. <https://doi.org/10.1016/j.matlet.2019.126574>.
- Li H, Lin F, Wang H, Wu H, Yang Y, Yu L, et al. Enhanced thermal stability and wettability of an electrospun fluorinated poly(aryl ether ketone) fibrous separator for lithium-ion batteries. *New J Chem* 2020;44(10):3838–46. <https://doi.org/10.1039/C9NJ05656D>.
- Wang C, Zhou Y, Shen B, Zhao X, Li J, Ren Q. Proton-conducting poly(ether sulfone ketone)s containing a high density of pendant sulfonic groups by a convenient and mild post-sulfonation. *Polym Chem* 2018;9(40):4984–93. <https://doi.org/10.1039/C8PY00996A>.
- Liao J, Wang J, Liu Z, Ye Z. Polar benzimidazole-containing (sulfonated) poly(arylene ether ketone)s as bifunctional binders for lithium-sulfur battery cathodes with high sulfur loadings. *ACS Appl Energy Mater* 2019;2(9):6732–40. <https://doi.org/10.1021/acsae.9b01214>.
- Xu J, Zhang Z, Yang K, He W, Yang X, Du X, et al. Construction of new transport channels by blending POM-based inorganic-organic complex into sulfonated poly(ether ketone sulfone) for proton exchange membrane fuel cells. *J Membrane Sci* 2020;596:117711. <https://doi.org/10.1016/j.memsci.2019.117711>.
- Lu P, Hsieh YL. Multiwalled Carbon Nanotube (MWCNT) reinforced cellulose fibers by electrospinning. *ACS Appl Mater Inter* 2010;2(8):2413–20. <https://doi.org/10.1021/am1004128>.
- Kuk E, Ha YM, Yu J, Im IT, Kim Y, Jung YC. Robust and flexible polyurethane composite nanofibers incorporating multi-walled carbon nanotubes produced by solution blow spinning. *Macromol Mater Eng* 2016;301(4):364–70. <https://doi.org/10.1002/mame.201500298>.
- Liu LY, Zhang ZX, Gou XF. Thermal conductivity of aligned CNT-polyethylene nanocomposites and correlation with the interfacial thermal resistance. *Polym Composite* 2020;41:1–11. <https://doi.org/10.1002/pc.25676>.